Influence of interannual variability in estimating the rate and acceleration of present-day global mean sea level

Lorena Moreira, Anny Cazenave, Hindumathi Palanisamy

Global and Planetary Change 199 (2021) 103450

Contents lists available at ScienceDirect

Global and Planetary Change

journal homepage: www.elsevier.com/locate/gloplacha

Research article

Influence of interannual variability in estimating the rate and acceleration of present-day global mean sea level

Lorena Moreira [a,*], Anny Cazenave [a,b], Hindumathi Palanisamy [c]

[a] International Space Science Institute (ISSI), Bern, Switzerland
[b] Laboratoire d'Etudes en Geophysique et Oceanographie Spatiales (LEGOS), Toulouse, France
[c] Centre for Climate Research Singapore, Meteorological Service Singapore, Singapore

ARTICLE INFO

Keywords:
Sea level rise
Sea level rate
Sea level acceleration
Interannual variability
Climate modes

ABSTRACT

Recent studies have shown that the global mean sea level (GMSL) is accelerating. For improved process understanding and sea level projections, it is crucial to precisely estimate the GMSL acceleration due to externally-forced global climate change. For that purpose, the internal climate variability-related signal of the GMSL needs to be removed from the GMSL record. In the present study, we estimate how the observed GMSL rate has evolved with time over the altimetry era (1993-present), with the objective of determining how it is influenced by the interannual variability. We find that the GMSL rate computed over 5-year moving windows, displays significant interannual variability around 6–7 years and 12–13 years, preventing from robust acceleration estimation. To remove from the observed GMSL time series, the interannual variability, possibly related to internal climate modes, like ENSO, PDO, IOD, NAO or AMO, we use two methods previously widely applied in the literature: (1) multiple linear regression of the GMSL against some climate indices, and (2) Empirical Orthogonal Function (EOF) decomposition of the gridded sea level data to isolate the interannual signal. Although the interannual signal of the corrected GMSL time series is reduced, a cycle around 6–7 years still remains in the GMSL rate. We discuss possible sources of the remaining 6-7-year cycle, including the limitation of the methods used to remove the interannual variability.

1. Introduction

Until recently, it was believed that the global mean sea level (GMSL) had risen almost linearly during the altimetry era (since 1993). However recent studies based on the TOPEX/Poseidon and Jason altimetry missions, accounting for the instrumental drift of the onboard altimeter of the TOPEX/Poseidon satellite (Watson et al., 2015; Beckley et al., 2017; Ablain et al., 2017), have shown that the GMSL is accelerating (Watson et al., 2015; Dieng et al., 2017; Yi et al., 2017; Nerem et al., 2018; Von Schuckmann et al., 2020), a result confirmed by other altimetry missions such as ERS-1 & 2 and Envisat (Veng and Andersen, 2020), and also by tide-gauge records (Dangendorf et al., 2019).

However, the altimetry-based GMSL record, more than 27-year long, is also impacted by interannual/decadal variability due to internal climate modes of the coupled ocean-atmosphere system. Previous studies have shown in particular that the terrestrial water storage and ocean thermal expansion components of the GMSL budget display a strong interannual variability related to El Niño-Southern Oscillation (ENSO) (Nerem et al., 2010; Boening et al., 2012; Fasullo et al., 2013; Cazenave et al., 2014; Piecuch and Quinn, 2016; Hamlington et al., 2019, 2020). Separating the respective contributions of internal climate variability and external forcing factors, in particular those due to human-induced global warming, to present-day global mean sea level rise is a major issue for improved detection of the global mean sea level acceleration, process understanding and precise modelling of future sea level variations.

In this study, we estimate the temporal evolution of the GMSL rate, firstly using the observed altimetry-based time series (January 1993 to December 2019), and secondly after removing the interannual variability in the GMSL using two methods:

1. The multiple linear regression method (called hereinafter method 1) (e.g., Zhang and Church, 2012), consisting of regressing the GMSL time series with respect to the main climate modes such as MEI (Multivariate ENSO Index), PDO (Pacific Decadal Oscillation), IOD

* Corresponding author.
E-mail address: lorena.moreira@issibern.ch (L. Moreira).

https://doi.org/10.1016/j.gloplacha.2021.103450
Received 9 September 2020; Received in revised form 8 January 2021; Accepted 6 February 2021
Available online 10 February 2021

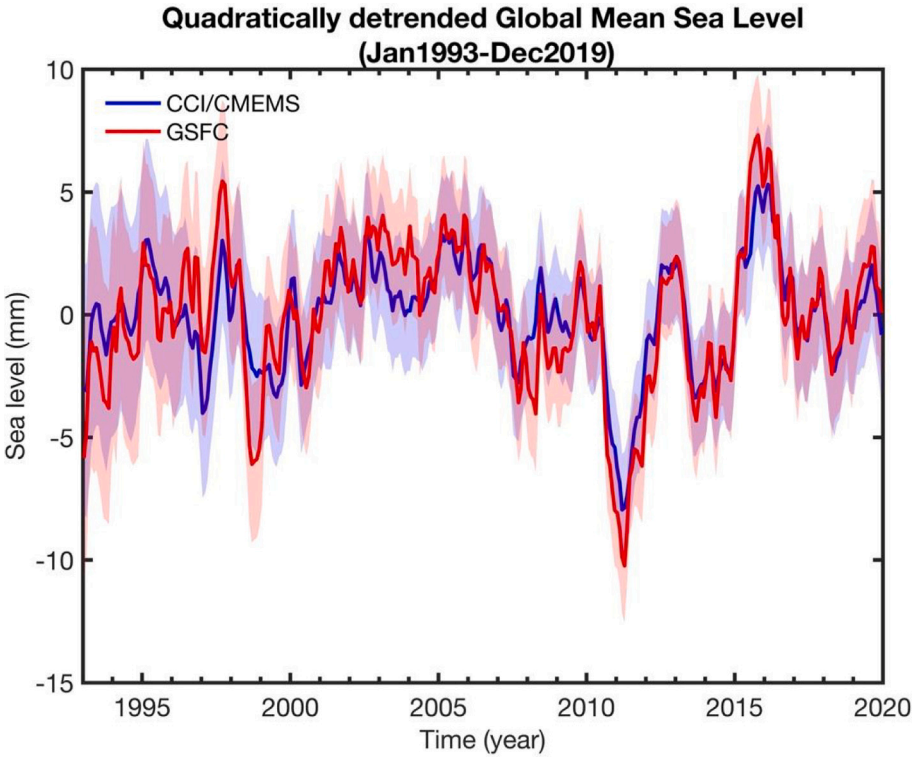

Fig. 1. Quadratically detrended GMSL time series over 1993–2019 for the CCI/CMEMS GMSL (blue curve) and GSFC GMSL (red curve). The shaded areas represent the GMSL uncertainty at 90% confidence level. (For interpretation of the references to colour in this figure legend, the reader is referred to the web version of this article.)

(Indian Ocean Dipole), NAO (North Atlantic Oscillation) and AMO (Atlantic Meridional Oscillation).

2. The EOF method (called method 2) (Han et al., 2017) consisting of isolating the EOF modes of gridded sea level data that are related to the interannual variability.

We then recompute the rate of the corrected GMSL and its evolution through time and compare the results obtained by each of the two methods.

2. Data

2.1. Altimetry-based sea level data

Two sources of data have been used:

1. The Climate Change Initiative (CCI) sea level product (http://www.esa-sealevel-cci.org) from the European Space Agency (ESA) from January 1993 to December 2015 (version 2.0). This product combines data from the TOPEX/Poseidon, Jason-1/2, GFO, ERS-1/2, Envisat, CryoSat-2 and SARAL/Altika altimetry missions and is based on a new processing system with dedicated algorithms and adapted data processing strategies (Legeais et al., 2018). It is available as a gridded 1/4° x 1/4° data set over 82°N and 82°S latitudinal range. This time series has been extended as of January 2016 by sea level data from CMEMS (Copernicus Marine Environment Monitoring Service) (http://marine.copernicus.eu/). The TOPEX-A instrumental drift due to aging of the TOPEX-A altimeter placed in the TOPEX/Poseidon mission from January 1993 to early 1999 has been corrected, applying the correction proposed by Ablain et al. (2017). This consists of removing a trend of −1.0 mm/yr over January 1993 to July 1995 and + 3.0 mm/yr over August 1995 to February 1999. The glacial isostatic adjustment (GIA) correction is applied (a value of −0.3 mm/yr is considered, Peltier, 2004).
2. The sea level data from the Goddard Space Flight Center (GSFC) (https://sealevel.nasa.gov/understanding-sea-level/key-indicators/global-mean-sea-level/). The GSFC data set is based on the TOPEX/Poseidon, Jason-1, Jason-2 and Jason-3 data averaged over the 66°S - 66°N domain directly from the along-track sea surface height data. To account for the TOPEX-A altimeter drift, the internal calibration-mode range correction, included in the TOPEX 'net instrument' correction, (supposed to be suspect owing to changes in the altimeter's point target response) has been suppressed from the GSFC data set (Beckley et al., 2017). It is also corrected for GIA, considering a value of −0.3 mm/yr.

The GMSL data sets have been analysed over January 1993 to December 2019, i.e., a complete 27-yr long time span.

Being interested in the GMSL interannual variability and long-term trend, we removed the annual and semi-annual signals to each time series, through a least-squares fit of 12- and 6-month periods. For some of the analyses presented below, the GMSL time series have been quadratically detrended to highlight the interannual variability.

2.2. Climate modes

In this study, we considered the following climate indices: MEI, PDO, IOD, NAO and AMO.

MEI is the Multi variate ENSO index representing El Niño Southern Oscillation. It combines information of surface pressure, sea surface temperature, surface wind and outgoing long-wavelength radiation over the tropical Pacific. PDO and IOD are derived from sea surface temperature data, respectively north of 20°N in the Pacific, and over the Indian Ocean. NAO is defined by the sea level pressure difference between Azores and Iceland, while AMO represents the average sea surface temperature of the North Atlantic Basin. The corresponding time series have been downloaded from publicly accessible data websites (date of download: 22 December 2020):

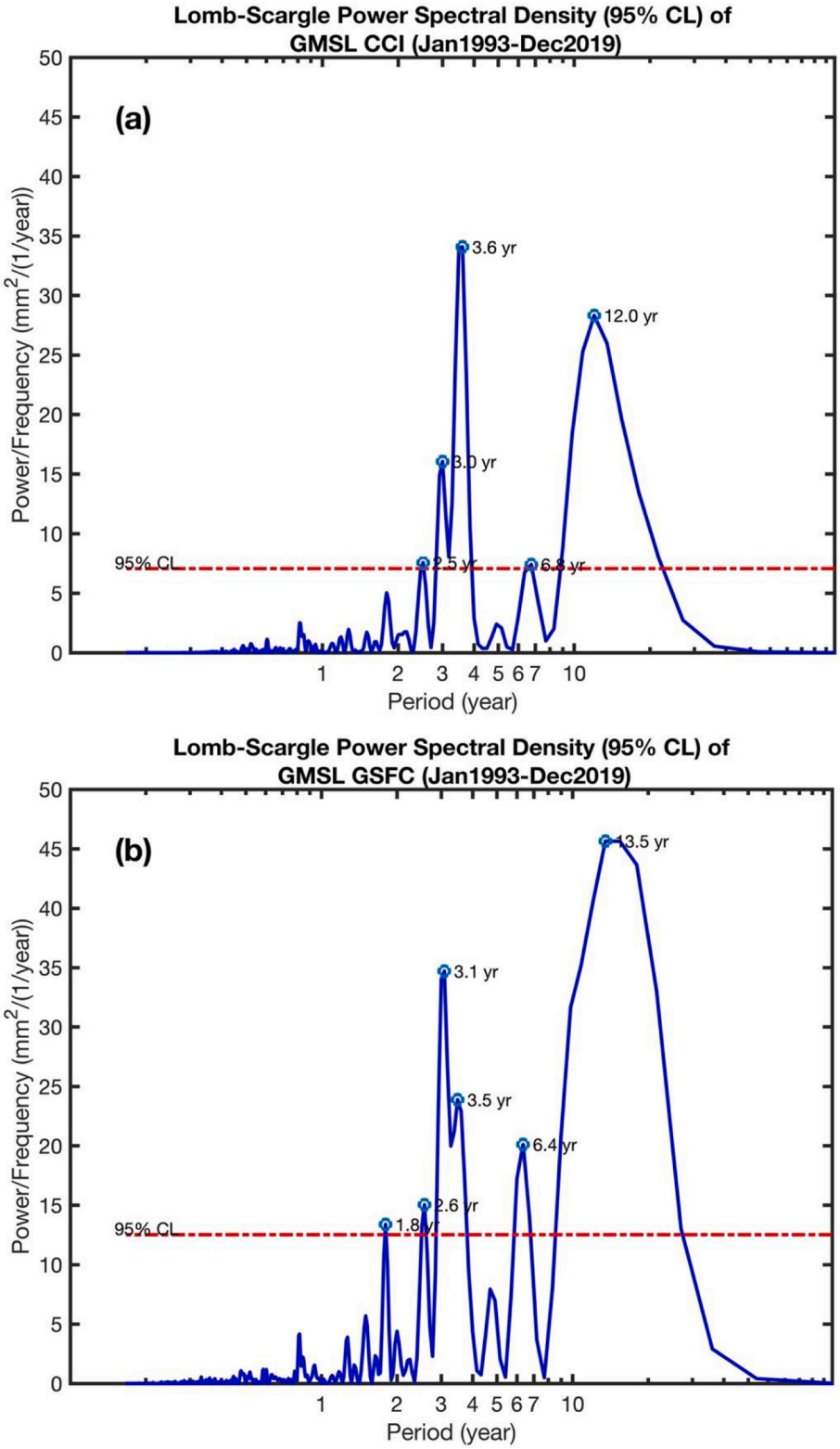

Fig. 2. Periodogram of the initial quadratically detrended GMSL time series over 1993–2019. (a): CCI/CMEMS; (b) GSFC. The 95% confidence level (noted CL) is shown by the horizontal dashed line.

MEI: https://psl.noaa.gov/enso/mei/data/meiv2.data
PDO: https://www.ncdc.noaa.gov/teleconnections/pdo/
IOD: https://psl.noaa.gov/gcos_wgsp/Timeseries/DMI/
NAO: https://www.cpc.ncep.noaa.gov/products/precip/CWlink/pna/nao.shtml
AMO: https://psl.noaa.gov/data/timeseries/AMO/

The time span January 1993 to December 2019 has been considered for the climate indices, as for the GMSL time series. For further analyses, in the climate index time series we removed 6- and 12-month cycles through a least-squares fit. For the computation of the power spectrum densities, a trend has been removed and a 3-month smoothing has been performed.

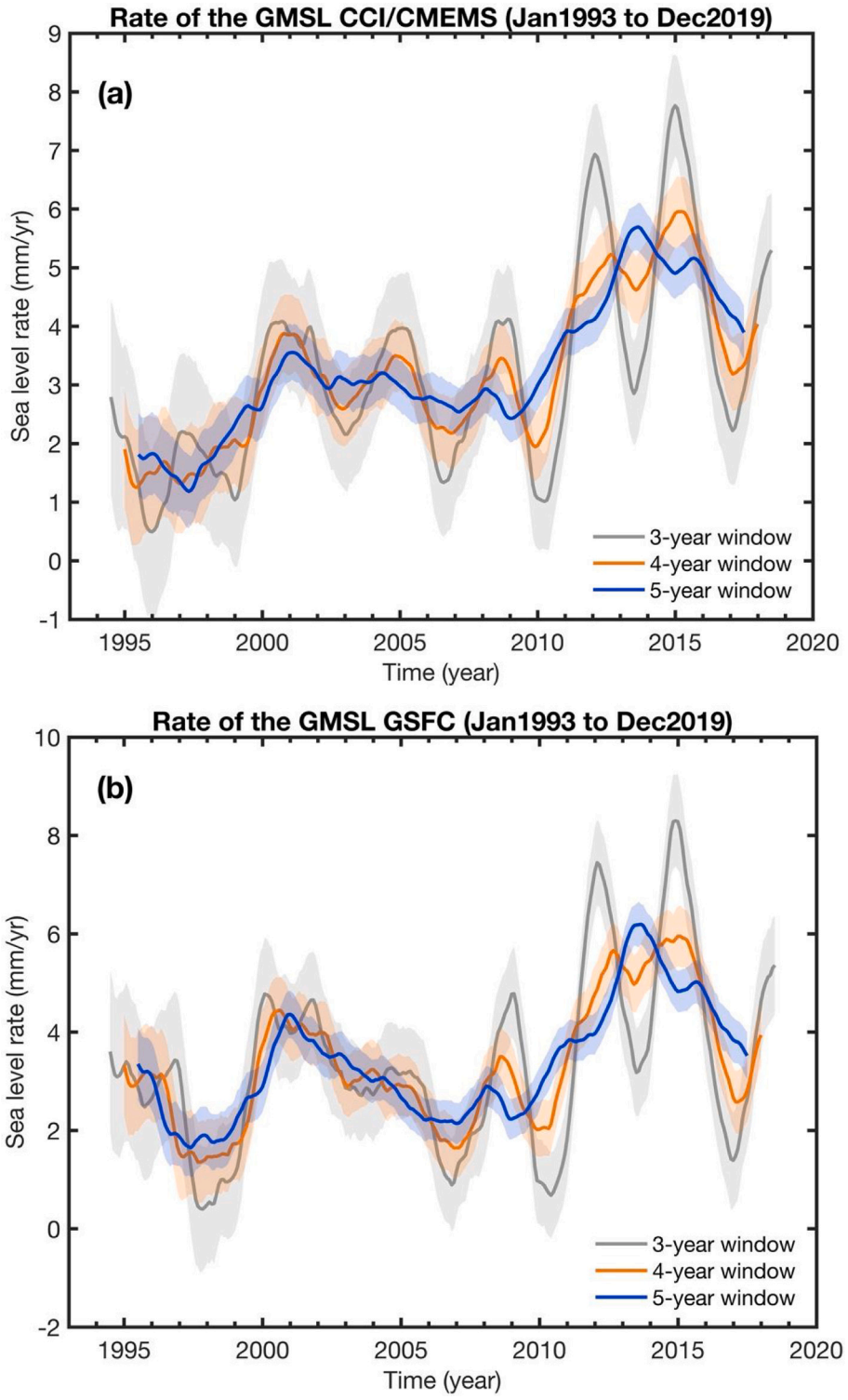

Fig. 3. GMSL rate computed over 3-year, 4-year and 5-year windows shifted by 1-month (grey, orange and blue curves respectively). The shaded areas represent the rate uncertainty at 95% confidence level. Panels (a) and (b) correspond to the CCI/CMEMS and GSFC rates respectively. (For interpretation of the references to colour in this figure legend, the reader is referred to the web version of this article.)

2.3. Interannual variability of the observed GMSL and associated GMSL rate

We first show the quadratically detrended (QD) GMSL time series over January 1993–December 2019 for the CCI/CMEMS and GSFC data sets (Fig. 1). We note that the two curves agree reasonably well but the CCI/CMEMS curve displays in general lesser amplitude during extremes, as a result of the 3-month smoothing applied to this data set (Legeais et al., 2018). The year-to-year fluctuations are highly correlated with MEI, hence with the occurrence of ENSO events, as shown in many previous studies (e.g., Nerem et al., 2010; Cazenave et al., 2014). The uncertainties of the GMSL presented here are based on Ablain et al. (2019), and are reported with a 90% confidence level. The latter study considers three types of errors: (a) biases in the GMSL between

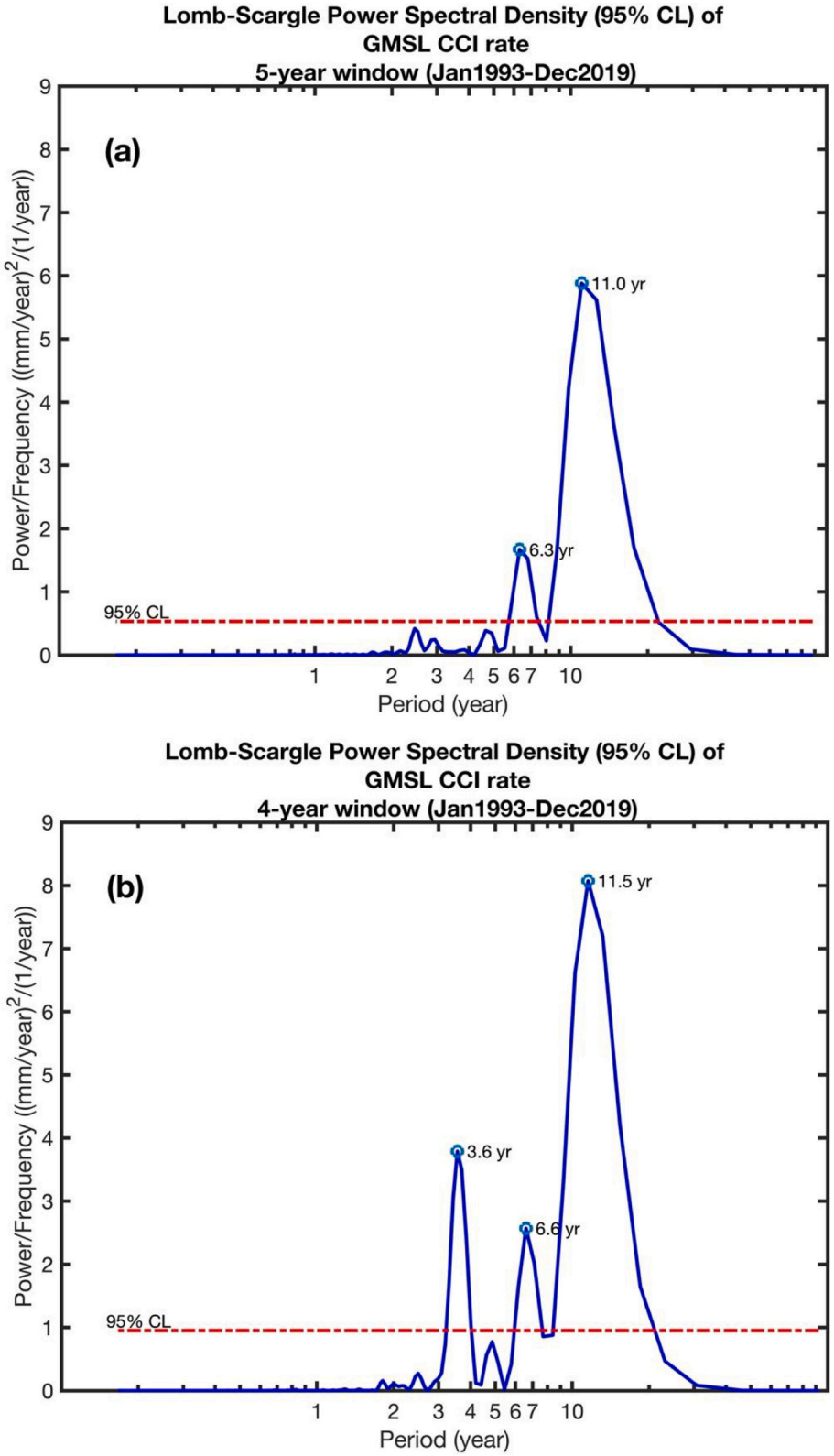

Fig. 4. Periodograms of the GMSL rate computed over 5-year (a) and 4-year (b) windows shifted by 1-month, considering the 1993-2019-time span for the CCI/CMEMS GMSL. The 95% confidence level (noted CL) is shown by the horizontal dashed line.

successive altimetry missions, characterized by bias uncertainties at a given time; (b) drifts in GMSL characterized by a trend uncertainty; and (c) other measurement errors which exhibit temporal correlations. These time-correlated residual errors are characterized by their standard deviation and by the correlation timescale (Ablain et al., 2019).

We next investigate the dominant periodicities of the two QD GMSL time series (Fig. 2). For that purpose, we have used the Lomb-Scargle periodogram. The Lomb-Scargle periodogram is a method that allows efficient computation of a Fourier-like power spectrum estimator for detecting and characterizing periodic signals in unevenly sampled data

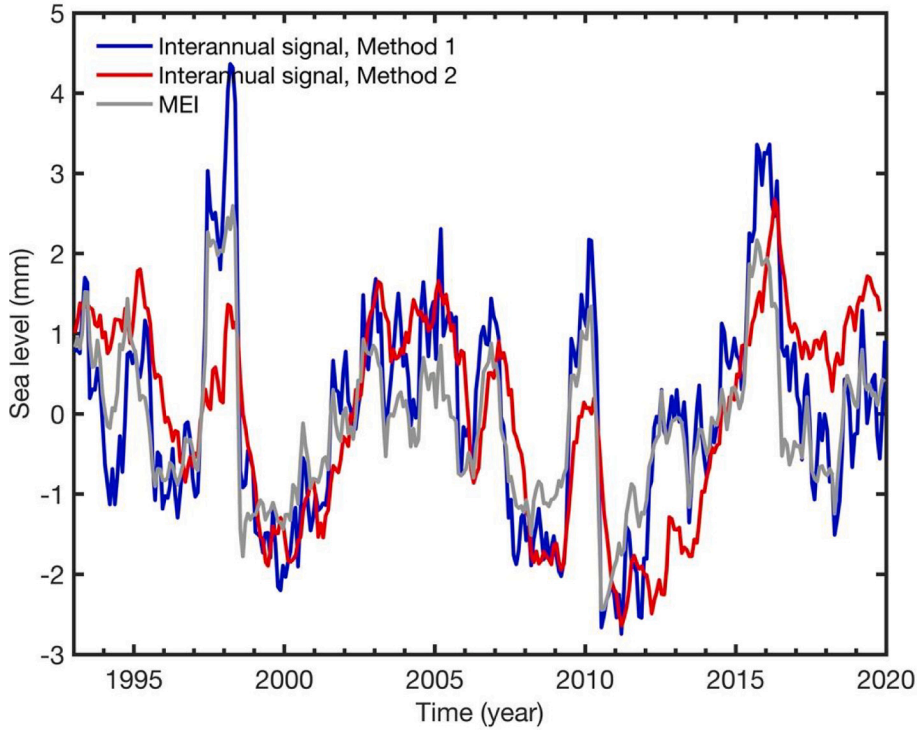

Fig. 5. Interannual signal removed from the original GMSL (CCI/CMEMS data) using method 1 (blue curve) and method 2 (red curve). The MEI index is superimposed (grey curve). (For interpretation of the references to colour in this figure legend, the reader is referred to the web version of this article.)

(e.g., VanderPlas, 2018). We use the plomb function provided by MATLAB to calculate the power spectral density estimate of the quadratically detrended time series of interest. As sample rate, we consider 12 samples per year. We represent the logarithm of the multiplicative inverse of the frequency, which is the period in years. We also estimate probability of detection of the estimated period, that measures the peak significance level. We set the threshold at the 95% confidence level. The detection probability shows the probability that a peak in the spectrum is not due to random fluctuations.

Fig. 2 displays dominant peaks around 3 years and 12–13 years. The GSFC periodogram also shows a peak at 6–7 year, that is only barely significant in the CCI/CMEMS spectrum.

Since our initial objective was to investigate how the GMSL rate evolves with time, we next compute the GMSL rate over successive 3-year, 4-year and 5-year windows shifted by 1-month, considering both the CCI/CMEMS and GSFC data sets. The corresponding curves are shown in Fig. 3.

The rate uncertainty estimation is based on the Deming regression (Deming, 1943; Wu and Yu, 2018) in which a linear fit is computed accounting for the uncertainties of the variables, in our case the uncertainty in the GMSL proposed by Ablain et al. (2019). The best slope and intercept are computed by minimizing the chi-square calculated using both standard deviation on the dependent and independent variables. The uncertainty of the fitted parameters is computed using a Monte Carlo simulation with 1000 iterations, assuming that errors are Gaussian and centered. The algorithm used can be freely downloaded from the MATLAB Central File Exchange (https://www.mathworks.com/matlabcentral/fileexchange/45711-linear-fit-with-both-uncertainties-in-x-and-in-y) (retrieved 31 December 2020). Note that all uncertainties reported in the rates are given at the 1.96-sigma level, i.e., 95% confidence level.

For each data set, we note that the three curves (corresponding to the 3-year, 4-year and 5-year windows) show an overall similar behaviour, i.e., an irregular increase with time along with steep increases in 1995–2001 and 2009–2014. The 3-year window case displays much higher interannual oscillations, as expected.

In Fig. 4 are shown the periodograms of the QD (initial) GMSL rate for the 4-year and 5-year windows (only the CCI/CMEMS time series is considered here).

For both the 4-year and 5-year windows, the GMSL rate shows significant peaks around 6 years and 11–12 years.

2.4. Removal of the interannual variability of the GMSL

The presence of the strong interannual variability signal in the GMSL rate may prevent from accurately estimating trend and acceleration of the GMSL. Therefore, it is important to remove it from the GMSL before computing the rate and its evolution through time (e.g., Cazenave et al., 2014; Nerem et al., 2018). In the present study, this is done by removing the interannual signal using two different methods, as described below.

2.5. Method 1 (Regression method)

This method has been applied in several studies (e.g., Zhang and Church, 2012, Palanisamy et al., 2015) and references therein). The method consists of computing a linear regression of the GMSL time series with respect to an ENSO-related climate index (usually MEI). In effect, as shown in the literature (e.g., Nerem et al., 2010; Cazenave et al., 2014), the dominant source of interannual variability in the GMSL is due to ENSO. But other climate modes also influence the GMSL (e.g., Zhang and Church, 2012). Hence, additional climate indices should be considered at the same time, e.g., PDO, IOD, NAO and AMO:

$$GMSL(t) = a_0 + a_1 t + a_2 t^2 + a_3 MEI(t) + a_4 PDO(t) + a_5 IOD(t) + a_6 NAO(t) + a_7 AMO(t) \quad (1)$$

In Eq. (1) above, t is time. The least-squares fit consists of estimating the a_0 to a_7 coefficients. We applied this approach to the CCI/CMEMS time series. Note that for this computation the climate index times series are not detrended (only seasonal cycles are removed). That part of Eq. (1) related to the climate indices has been further removed to the original GMSL time series. The corresponding removed signal is shown

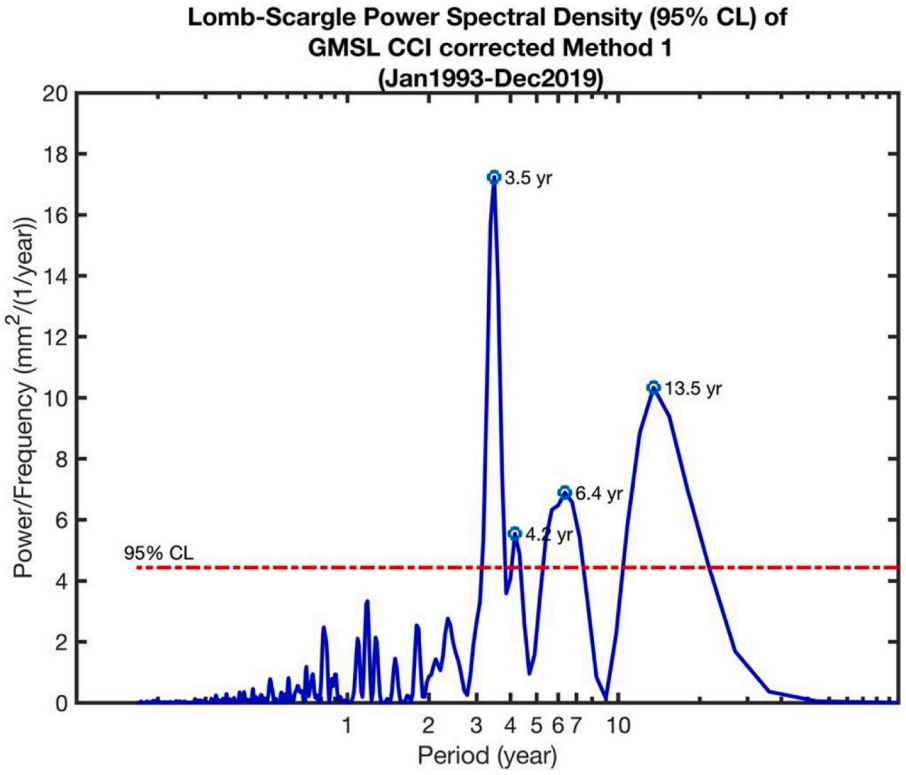

Fig. 6. Periodogram of the QD GMSL time series corrected for the regressed signal (method 1) over 1993–2019. The 95% confidence level (noted CL) is shown by the horizontal dashed line.

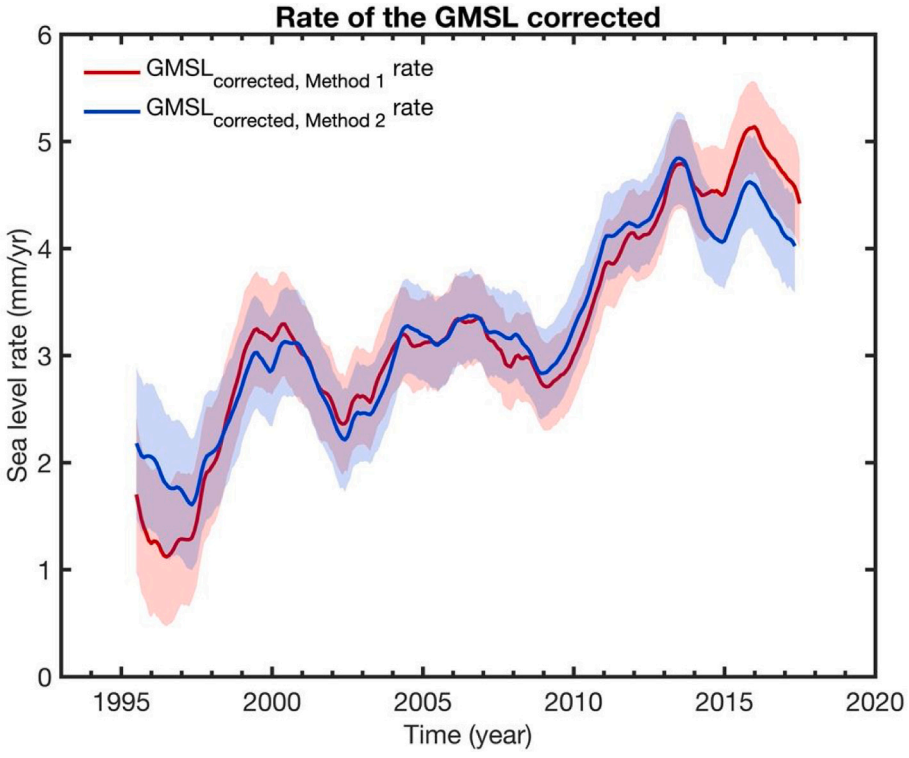

Fig. 7. GMSL rate (CCI/CMEMS data) over 5-year windows shifted by 1-month. Corrected GMSL (method 1; red curve); corrected GMSL (method 2; blue curve). The shaded areas represent the rate uncertainty at 95% confidence level. (For interpretation of the references to colour in this figure legend, the reader is referred to the web version of this article.)

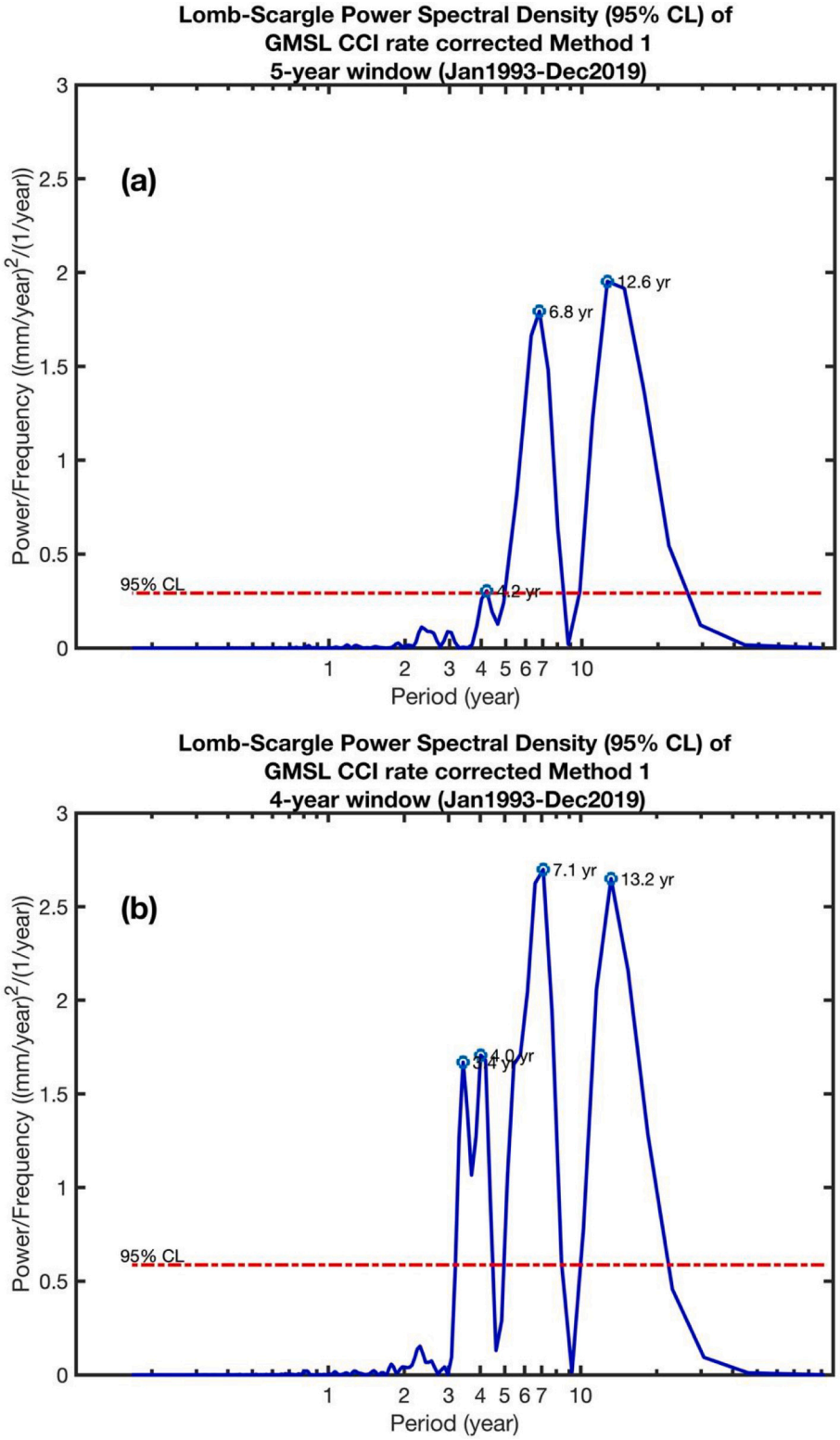

Fig. 8. Periodogram of the corrected GMSL rate (method 1). (a) 5-year window; (b) 4-year window. The 95% confidence level (noted CL) is shown by the horizontal dashed line.

in Fig. 5.

The interannual signal removed from the GMSL by method 1 is highly correlated with the MEI index, with a correlation of 0.91. The computed regression coefficients are $a_{3,\ MEI} = 1.39$, $a_{4,\ PDO} = 0.11$, $a_{5,\ IOD} = -0.92$, $a_{6,\ NAO} = 0.07$, and $a_{7,\ AMO} = 2.88$. We next removed the regressed signal shown above to the initial GMSL. Fig. 6 shows the periodogram of the QD GMSL (CCI/CMEMS dataset) corrected for the regressed signal.

Compared to Fig. 2a (periodogram of the initial QD GMSL), the amplitude of the 3-yr peak has decreased, but the peak is still there. A similar comment can be made for the 12-13-yr peak. On the other hand, the 6-7-yr peak barely significant in the initial GMSL is now well above

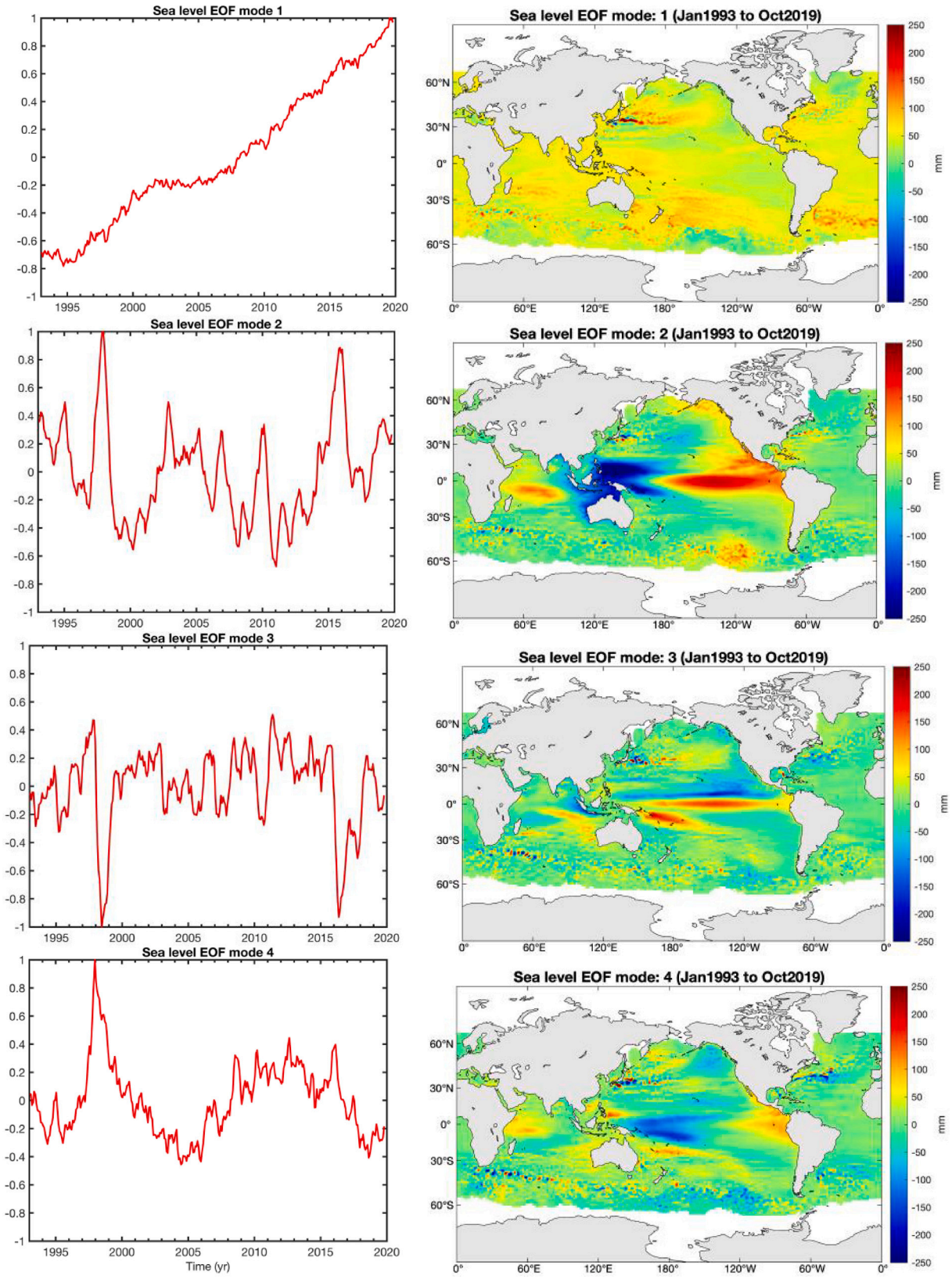

Fig. 9. Modes 1, 2, 3 and 4 of the EOF decomposition of the C3S gridded sea level time series over 1993–2019. Principal components and associated spatial patterns are shown in the left and right panels respectively.

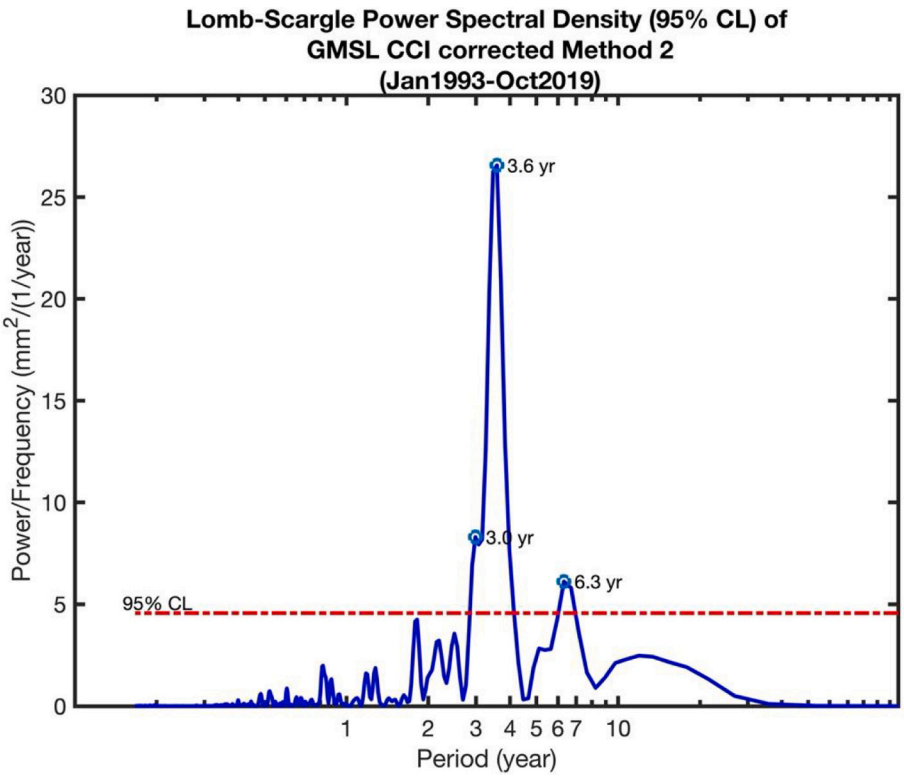

Fig. 10. Periodogram of the QD GMSL time series corrected for the interannual signal (method 2) over January 1993–October 2019. The 95% confidence level (noted CL) is shown by the horizontal dashed line.

the 95% confidence level. Note that to check the robustness of the results, we reproduced the above computation using the Hilbert transforms of the climate indices. Similar results were obtained (not shown). In particular the same peaks as those seen in Fig. 6 are found, with the same level of confidence.

We next recomputed the GMSL rate after correcting for the interannual variability by method 1. The corrected GMSL rate is shown in Fig. 7 for the 5-yr moving window case.

Compared to the original GMSL rate, we note some difference in the evolution with time of the corrected GMSL rate. The step like behaviour seen in the uncorrected GMSL rate (Fig. 3a) is less visible. Rather, we note a long-term increase in the rate on which is superimposed some interannual variability. The periodogram of the corrected GMSL rate (method 1; 5-year window) is shown on Fig. 8a. The spectrum shows two peaks at 6–7 years and 12–13 years.

To check whether the 6-7-year peak is not an artifact of the 5-year window choice, we also show the same spectrum but considering a 4-year window for computing the rate (Fig. 8b). We still see the two significant peaks around 7-year and 13-year, indicating that the 6–7-year cycle seen in Fig. 8a does result from some aliasing related to the 5-yr window choice.

What is the origin of the 6-7-yr and 13-yr cycles in the corrected GMSL rate? Are they unrelated to the dominant climate indices considered here? Or do they result from an imperfect removal of the interannual variability by method 1? The next section intends to address the second option by considering a different approach.

2.6. Method 2 (EOF decomposition)

Another method widely used in the literature to remove the interannual variability in the GMSL is to apply an EOF decomposition to GMSL grids in order to isolate the modes related to the main climate indices, in particular ENSO. Some variant of this method has been developed. For example, Hamlington et al. (2019) employ a cyclostationary empirical orthogonal function (CSEOF) analysis (Kim et al., 2015). As in the EOF, the CSEOF method decomposes space-time data into a series of modes that consist of a spatial component and a corresponding temporal component but the main difference with the EOF is that the spatial component is time dependent, which allows the spatial pattern of each CSEOF mode to vary in time, with the temporal evolution of the spatial pattern constrained to be periodic with a selected "nested period". Hamlington et al. (2019) argue that CSEOF is superior to the classical EOF for two reasons: (1) no need to target a specific climate signal, and (2) CSEOFs allow for temporally lagged covariation between different climate variables that may be otherwise difficult to extract. This last point is particularly important when simultaneously analysing multiple variables. However, a limitation of this method is the need to select a nested period prior to performing the analysis.

Here we apply the widely used EOF decomposition (e.g., Han et al., 2017), considering that the two methods provide essentially similar results.

We used gridded sea level time series provided by the Copernicus Climate Change Service (C3S) downloaded from https://climate.copernicus.eu/ESOTC/2019/sea-level, over January 1993 to October 2019 (the last available date at the time of downloading), and computed the dominant modes of the EOF decomposition. Fig. 9 shows the first four modes of the EOF decomposition of the gridded GMSL data.

The first mode shows the well- known spatial trend patterns in sea level (e.g., Legeais et al., 2018). It explains 14.5% of the total variance. Modes 2, 3 and 4, which explain 11.43% of the total variance, display ENSO signatures in the Pacific Ocean and IOD in the Indian Ocean (Han et al., 2019).

We further considered modes 2, 3 and 4, assuming they represent most of the interannual variability of the sea level signal. After combining the spatial component of each mode with the corresponding principal component, we geographically averaged the sea level signal associated with the 2nd, 3rd and 4th modes (applying an area

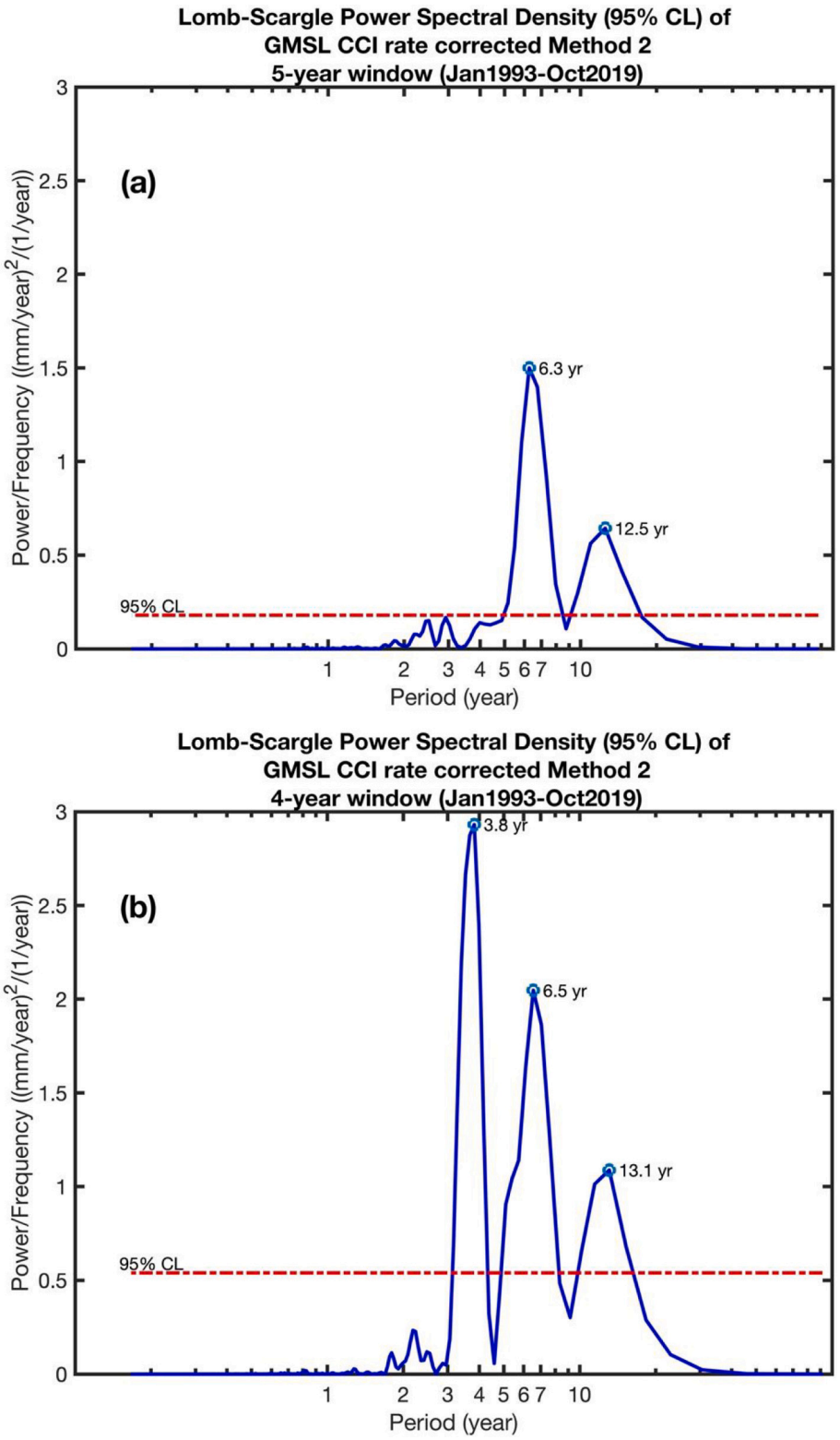

Fig. 11. Periodogram of the corrected GMSL rate (method 2) over January 1993 to October 2019. (a) 5-year window; (b) 4-year window. The 95% confidence level (noted CL) is shown by the horizontal dashed line.

weighting) and removed it from the original GMSL. The interannual signal associated with modes 2, 3 and 4 (method 2) is shown in Fig. 5. It correlates rather well with that of method 1, except during the 1997–1998 ENSO event. The correlation with MEI amounts 0.63.

The periodogram of the corrected GMSL (method 2) is shown in Fig. 10. It has a dominant peak at 3.6 year and a secondary one at 6.3 year, like the corrected GMSL (method 1) (Fig. 6). However, unlike the latter, the 13-yr peak is below the 95% confidence level.

We further computed the rate of the corrected GMSL (method 2) over 5-year windows shifted by 1 month (Fig. 7), as well as the corresponding periodogram (Fig. 11a). As for method 1, we also show the periodogram of the corrected GMSL rate (method 2) computed over 4-year windows

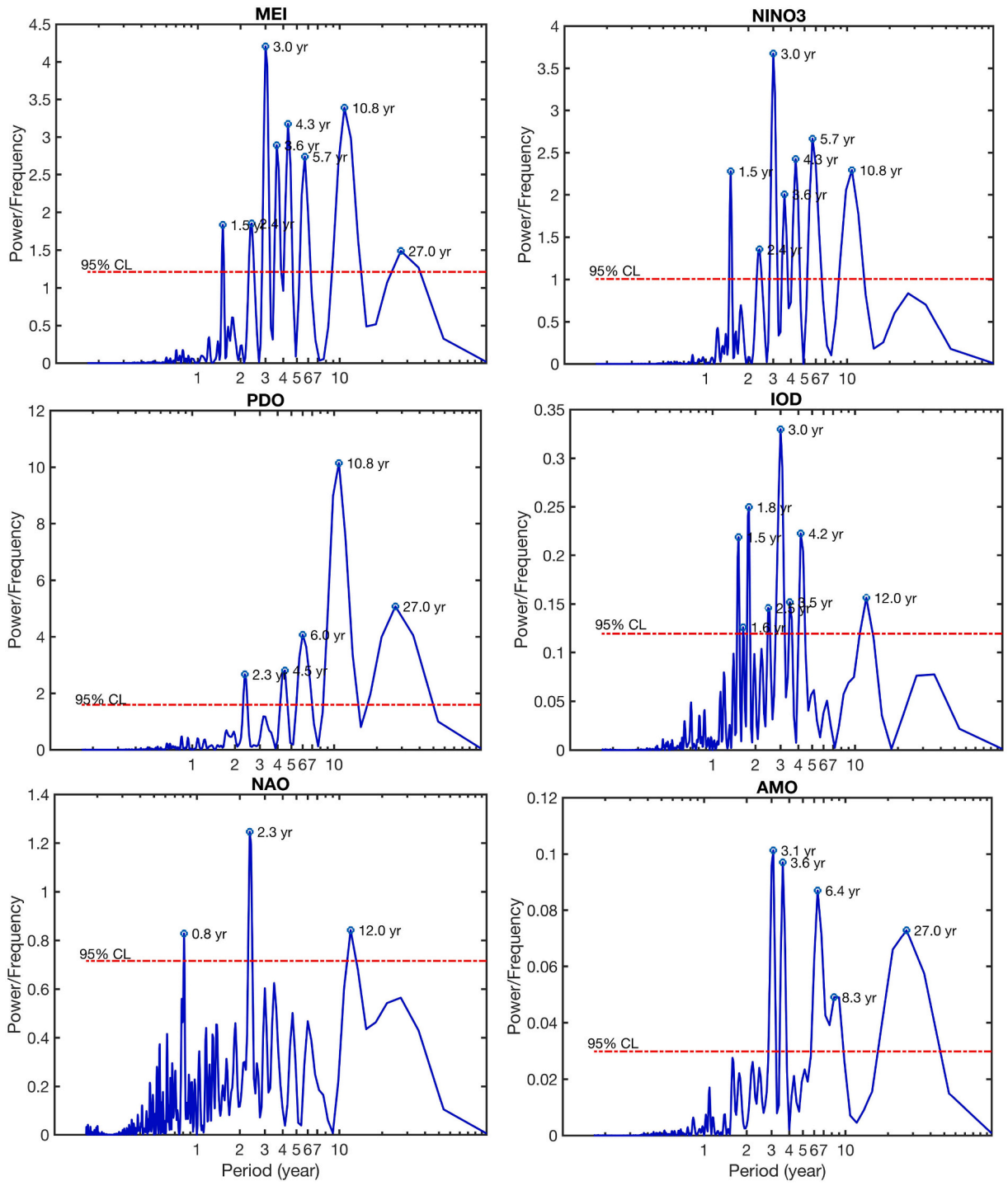

Fig. 12. Periodograms of the climate indices (MEI, Niño3.4, PDO, IOD, NAO and AMO) over January 1993–December 2019. The 95% confidence level (noted CL) is shown by the horizontal dashed line.

(Fig. 11b).

In both cases (5-year and 4-year windows), the spectrum of the corrected GMSL rate has a significant peak at 6–7 year, and a smaller one at 12–13 yr.

3. Discussion

In this study, we applied two methods to remove the interannual variability in the GMSL time series and in the GMSL rate. However, in both cases, there remains significant peaks at 6–7 years and to a lesser extent at 12–13 years. It is unlikely that such cycles are due to errors in the geophysical corrections applied to the altimetry data. In effect, Ablain et al. (2019) did not report any periodic errors at 6–7 years and 12–13 years in their GMSL budget error analysis. Similarly, aliasing effects caused by high-frequency signals incorrectly sampled by the 10-day or 35-day orbital cycles of altimetry missions cannot cause such interannual cycles (M. Ablain, personal communication, January 2021). Could they still be related to the internal climate variability imperfectly removed by the methods considered here? Fig. 12 shows the periodograms of the climate indices considered in section 2.5. The Nino-3.4 index (downloaded the 22 December 2020 from https://psl.noaa.gov/gcos_wgsp/Timeseries/Nino34/) is included in order to check how

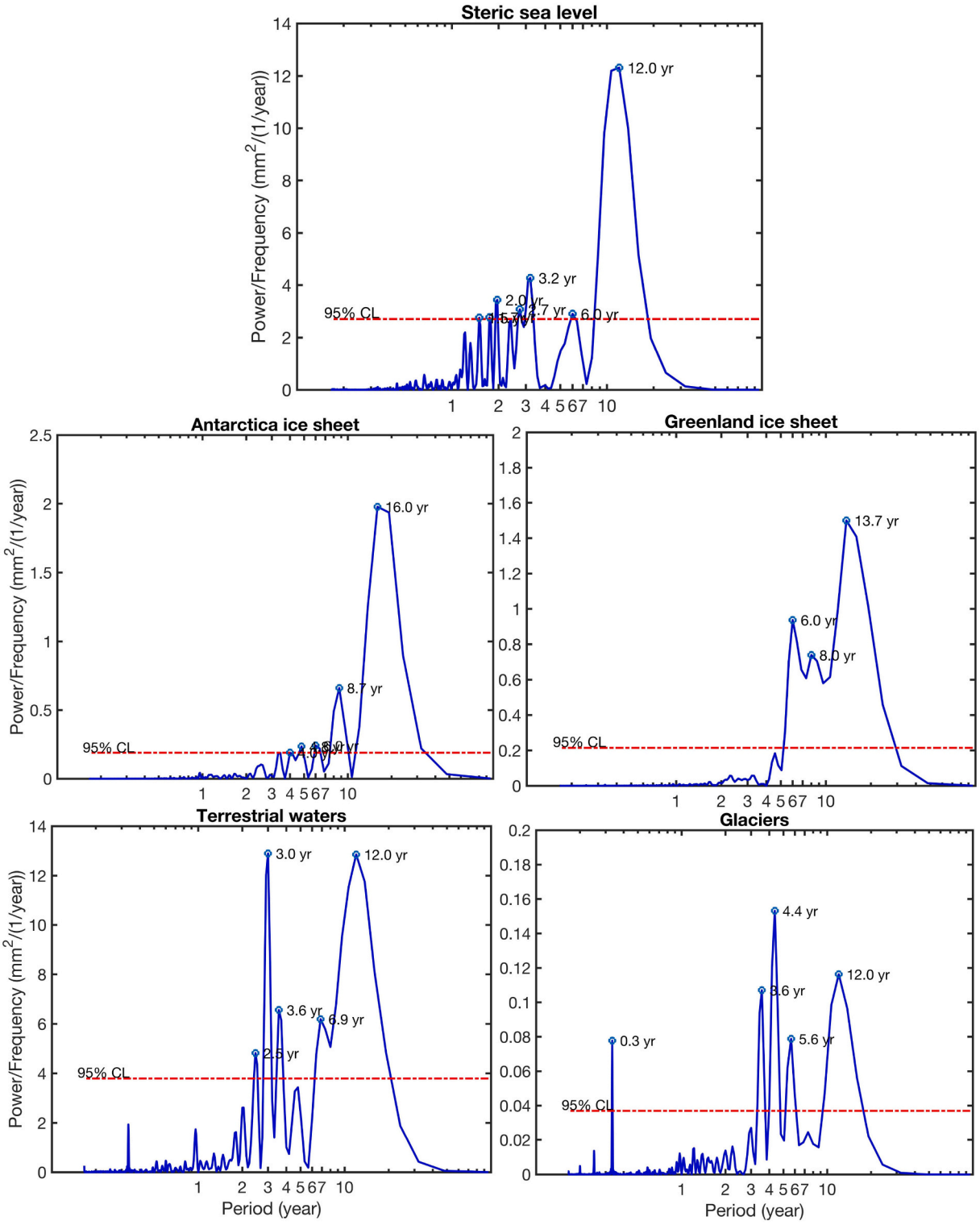

Fig. 13. Periodograms of the components of the sea level budget (steric sea level, Antarctica ice sheet, Greenland ice sheet, terrestrial waters and glaciers) from the Sea Level Budget Closure project of the ESA Climate Change Initiative over January 1993 to December 2016. The 95% confidence level (noted CL) is shown by the horizontal dashed line.

much its periodogram differs from that of MEI.

From Fig. 12, we note that several indices display significant energy around 6 year and 12 year. This is the case of MEI, PDO and NAO. AMO has a peak at 6–7 year but not at 12 year. Note that the power spectra of MEI and Niño3.4 are similar; thus, no need to also consider Niño3.4. It may well be that the two methods considered here imperfectly remove the GMSL interannual variability. In effect, in method 1, the regression to climate indices is defined from atmospheric and oceanic surface variables which are not necessarily appropriate to account for variations of the global mean sea level, an integrated quantity. Besides, method 1 implicitly assumes that the climate indices are independent. But studies have shown that is likely not the case. For example, García-García and

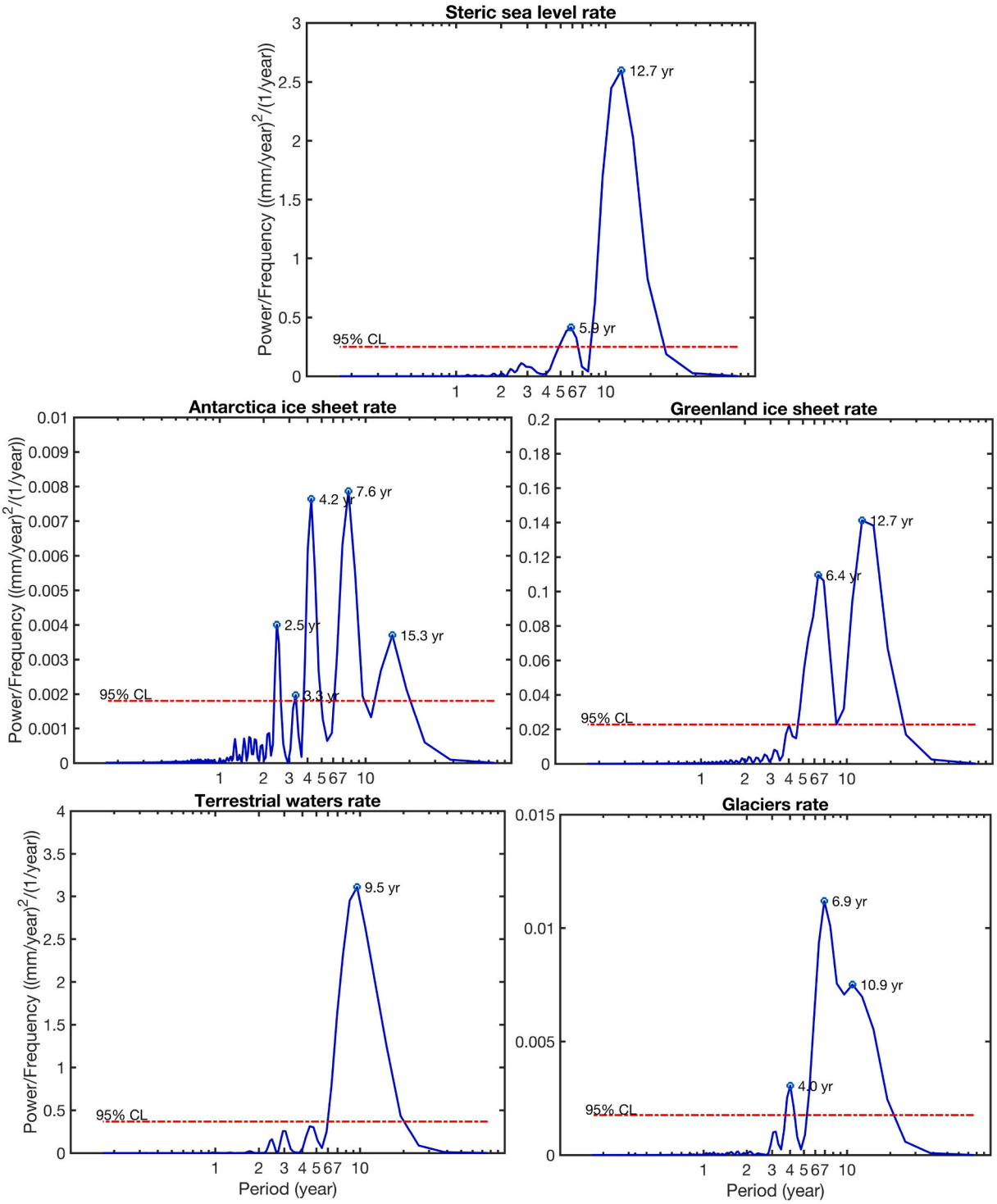

Fig. 14. Periodograms of the rates of the sea level budget components (steric sea level, Antarctica ice sheet, Greenland ice sheet, terrestrial waters and glaciers) from the Sea Level Budget Closure project of the ESA Climate Change Initiative over January 1993 to December 2016. The 95% confidence level (noted CL) is shown by the horizontal dashed line.

Ummenhofer (2015) indicate that AMO and ENSO are not independent entities, AMO modulating ENSO characteristics. Similarly, PDO and IOD are likely related to ENSO through non-linear interactions. Besides, the internal climate variability may be impacted by anthropogenic climate change but so far, no consensus exists between climate models about the effect of external forcing on the climate modes, in particular ENSO, as discussed in Cazenave et al. (2020)'s review.

Method 2 removes more interannual signal than method 1 (in particular the 12–13-year cycle) but not totally. It is possible that the separation between the different climate indices is imperfectly reflected by the modes computation, the interannual signal being possibly distributed in many more modes than considered here (note however that modes higher than 4 contain significant noise, hence considering more modes may be inappropriate). It is also possible that the interannual variability in the GMSL results from complex interactions of various signals affecting each component of the sea level budget (see below).

It is worth noting that a 6–7-year cycle is found in many variables of the Earth system, e.g., in the Earth's rotation, in the magnetic field, in crustal deformations, in the Earth's oblateness and other low-frequency terms of the Earth's gravity field (e.g., Abarca del Rio et al., 2000; Ding and Chao, 2018; Watkins et al., 2018; Chao and Yu, 2020, and references therein). While some of these 6-year fluctuations are attributed to Earth deep interior processes occurring in the core and at the core-mantle boundary (e.g., for the Earth's rotation and the magnetic field; e.g., Ding and Chao, 2018), for some other variables, climate-related processes occurring in the surface fluid envelopes or at the Earth's surface may rather be invoked. For example, the Earth's mean surface temperature, or separately the sea surface and land surface temperatures, display a clear cycle at 6-year period (not shown). A 7 cycle has been reported in the European surface temperature (Jajcay et al., 2016; Meyer and Kantz, 2019), possibly related to NAO.

While deep Earth processes are likely not responsible for the remaining cycles seen in the corrected GMSL rate, components of the GMSL (steric sea level, land ice melt, land water storage changes) partly driven by the internal variability of the climate system exhibit significant energy around 6–7 year and 12–13 year. This can be checked using the GMSL contributions computed over 1993–2016 by the Sea Level Budget Closure project of the ESA (European Space Agency) Climate Change Initiative (data freely available, downloadable at https://climate.esa.int/en/projects/sea-level/;Horwath et al., 2021). We considered the various data sets provided by this project for the steric sea level, glaciers, Greenland and Antarctica ice sheets and terrestrial water storage components, and computed their periodograms (Fig. 13) for the available 1993–2016-time span (i.e., shorter by 3 years than the time span of the present study). We also computed the periodograms of their rates (Fig. 14; 5-year windows). From Figs. 13 and 14, we note that, except the Antarctic ice sheet, components and their rates exhibit significant energy at 3–4-year, 6–7 year and 12–13 year. This is the case in particular of the steric sea level, a quantity integrating ocean temperature and salinity data over the upper ocean depth (down to 700 m up to 2004 and to 2000 m as of 2005). Its rate of change has two main cycles around 6 year and 12 year. A similar observation can be made for the glaciers and Greenland ice sheet rates. It is thus not really surprising that using climate indices defined by surface climate variables only, does not fully remove the whole interannual signal of the GMSL.

What this study indicates is that estimating the GMSL acceleration over the altimetry era is complex because of the remaining contamination of the interannual variability on this record of limited length (27 years). Our analysis shows that none of the two methods considered here is really superior to the other. The empirical removal of the signal related to climate indices (methods 1 and 2) leaves significant interannual variability in the corrected GMSL and its rate. However, method 2 better removes the 12–13-year signal than method 1.

The initial goal of this study was to provide a precise estimate of the change in rate of the GMSL over time, during the altimetry era, by removing the interannual variability. However, unexpectedly, two cycles at 6–7 year, and to a lesser extent at 12–13 year, still remain in the GMSL rate after empirically correcting for the interannual signal. How much does these residual cycles impact previous estimates of the GMSL acceleration remains unknown. Watson et al. (2015) found an acceleration of 0.037–0.041 mm/yr^2 over 1993–2014. Nerem et al. (2018) estimated the GMSL acceleration to 0.084 +/− 0.025 mm/yr^2 over 1993–2017 correcting for the Pinatubo eruption and removing the interannual variability applying the cyclostationary EOF approach. Yi et al. (2017) estimated the GMSL acceleration to be 0.27 +/− 0.17 mm/yr^2 over a short period (2005–2015). Veng and Andersen (2020) found a value of 0.095 +/− 0.009 mm/yr^2 over 1991–2019 and noted that account of Pinatubo eruption and ENSO effect on this time span lowers the acceleration by only 0.01 mm/yr^2, suggesting that extending the GMSL time series should minimize the interannual variability contamination. These published accelerations either are uncorrected for the interannual variability or account for ENSO only. Accounting for additional effects may provide slightly different acceleration estimates in view of the difficulty of robustly remove all sources of interannual variability affecting the GMSL.

Table 1
Accelerations estimated in this study for the original GMSL (CCI and GSFC data), corrected GMSL (CCI) for the two methods (errors are 1-sigma errors based on the least-squares fit), and published estimates.

	Acceleration (mm/yr^2)
$GMSL_{original}$ CCI/CMEMS	$a_{1993-2019} = 0.136 \pm 0.01$
$GMSL_{original}$ GSFC	$a_{1993-2019} = 0.102 \pm 0.01$
$GMSL_{corrected}$ CCI/CMEMS Method 1	$a_{1993-2019} = 0.129 \pm 0.01$
$GMSL_{corrected}$ CCI/CMEMS Method 2	$a_{1993-2019} = 0.115 \pm 0.01$
Watson et al. (2015)	$a_{1993-2014} = 0.041 \pm 0.058$
Yi et al. (2017)	$a_{2005-2015} = 0.27 \pm 0.17$
Nerem et al. (2018)	$a_{1993-2017} = 0.084 \pm 0.025$
Veng and Andersen (2020)	$a_{1991-2019} = 0.093 \pm 0.014$

This is summarized in Table 1 that gathers the accelerations estimated for the original GMSL, and corrected GMSL for the two methods (errors are 1-sigma errors based on the least-squares fit). Method 2 lowers the acceleration by 0.02 mm/yr^2 compared to the original value (same time interval, same time series). Table 1 also provide recently published acceleration estimates.

From Table 1, we conclude that empirically removing the internal variability as proposed in this study, as well as in Nerem et al. (2018) and in Veng and Andersen (2020), has finally a limited impact on the acceleration estimate. Extending the GMSL record will likely lead to more robust estimates of the sea level acceleration. Besides, more investigation is definitely needed to improve the methodology required to remove the interannual variability of the GMSL when estimating its acceleration.

Data availability

All data used in this study can be downloaded from the websites indicated in the data and discussion sections.

Author contributions

A. C. conceived the study. L. M. performed all analyses. All authors contributed to the writing of the paper and interpretation of the results.

Declaration of competing interest

All authors declare that there has no conflict of interest.

Acknowledgements

L. Moreira is supported by a post-doctoral fellowship from the International Space Science Institute (ISSI). We thank Hao Ding for interesting discussion about the 6-yr cycle found in several Earth system parameters.

References

Abarca del Rio, R., Gambis, D., Salstein, D.A., 2000. Interannual signals in length of day and atmospheric angular momentum. Ann. Geophys. 18, 347–364.

Ablain, M., Jugier, R., Zawadki, L., Taburet, N., 2017. The TOPEX-A Drift and Impacts on GMSL Time Series. AVISO Website. October 2017. https://meetings.aviso.altimetry.fr/fileadmin/user_upload/tx_ausyclsseminar/files/Poster_OSTST17_GMSL_Drift_TOPEX-A.pdf.

Ablain, M., Meyssignac, B., Zawadzki, L., Jugier, R., Ribes, A., Spada, G., Benveniste, J., Cazenave, A., Picot, N., 2019. Uncertainty in satellite estimates of global mean sea-level changes, trend and acceleration. Earth Syst. Sci. Data 11, 1189–1202. https://doi.org/10.5194/essd-11-1189-2019.

Beckley, B.D., Callahan, P.S., Hancock, D.W., Mitchum, G.T., Ray, R.D., 2017. On the 'Cal-Mode' correction to TOPEX satellite altimetry and its effect on the global mean

Sea Level Time Series. J. Geophys. Res. Oceans 122 (11), 8371–8384. https://doi.org/10.1002/2017jc013090.
Boening, C., Willis, J.K., Landerer, F., Nerem, S., Fasullo, J., 2012. The 2011 La Nina: so strong, the oceans fell. Geophys. Res. Lett. 39 https://doi.org/10.1029/2012GL053055. L19602.
Cazenave, A., Dieng, H.B., Meyssignac, B., von Schuckmann, K., Decharme, B., Berthier, E., 2014. The rate of sea-level rise. Nat. Clim. Chang. 4 (5), 358–361. https://doi.org/10.1038/nclimate2159.
Cazenave, A., Meehl, G., Montoya, M., Toggweiler, J.R., Claudia, Wieners C., 2020. Climate change and impacts on variability and interactions. In: Mechoso, Carlos R. (Ed.), Interacting Climates of Ocean Basins; Observations, Mechanisms, Predictability, and Impacts. Cambridge University Press, 358 pages, ISBN: 9781108492706, published November 2020.
Chao, B., Yu, Y., 2020. Variation of the equatorial moments of inertia associated with a 6-year westward rotary motion in the Earth. Earth Planet. Sci. Lett. 542, 116316.
Dangendorf, S., Hay, C., Calafat, F.M., et al., 2019. Persistent acceleration in global sea-level rise since the 1960s. Nat. Clim. Chang. 9, 705–710. https://doi.org/10.1038/s41558-019-0531-8.
Deming, W.E., 1943. Statistical Adjustment of Data. Wiley, NY, ISBN 0-486-64685-8 (Dover Publications edition, 1985).
Dieng, H.B., Cazenave, A., Meyssignac, B., Ablain, M., 2017. New estimate of the current rate of sea level rise from a sea level budget approach. Geophys. Res. Lett. 44 https://doi.org/10.1002/2017GL073308.
Ding, H., Chao, B., 2018. A 6-year westward rotary motion in the Earth: detection and possible MICG coupling mechanism. Earth Planet. Sci. Lett. 495, 50–55. https://doi.org/10.1016/j.epsl.2018.05.009.
Fasullo, J., Boening, C., Landerer, F., Nerem, R.S., 2013. Australia's unique influence on global sea level in 2010-2011. Geophys. Res. Lett. 40, 4368–4373. https://doi.org/10.1002/grl.50834.
García-García, D., Ummenhofer, C.C., 2015. Multidecadal variability of the continental precipitation annual amplitude driven by AMO and ENSO. Geophys. Res. Lett. 42, 526–535. https://doi.org/10.1002/2014GL062451.
Hamlington, B.D., Cheon, S.H., Piecuch, C.G., Karnauskas, K.B., Thompson, P.R., Kim, K.-Y., et al., 2019. The dominant global modes of recent internal sea level variability. J. Geophys. Res. Oceans 124, 2750–2768. https://doi.org/10.1029/2018JC014635.
Hamlington, B.D., Piecuch, C.G., Reager, J.T., Chandanpurkar, H., Frederikse, T., Nerem, R.S., Fasullo, J.T., Cheon, S.H., 2020. Origin of interannual variability in global mean sea level. Proc. Natl. Acad. Sci. 117 (25), 13983–13990. https://doi.org/10.1073/pnas.1922190117. June 23, 2020.
Han, W., Meehl, G.A., Stammer, D., Hu, A., Hamlinghton, B., Kenigson, J., Palanisamy, H., Thompson, P., 2017. Spatial patterns of sea level variability associated with natural internal climate modes. Surv. Geophys. 38, 217–250. https://doi.org/10.1007/s10712-016-9386-y.
Han, W., Stammer, D., Thompson, P., Ezer, T., Palanisamy, H., Zhang, X., Domingues, C. M., Zhang, L., Yuan, D., 2019. Impacts of basin-scale climate modes on coastal sea level: a review. Surveys in Geophysics 40 (6), 1493–1541. https://doi.org/10.1007/s10712-019-09562-8.
Horwath, M., Gutknecht, B.D., Cazenave, A., Palanisamy, H., et al., 2021. Global sea level budget and ocean mass budget, with focus on advanced data products and uncertainty characterization. Earth Syst. Sci. Data. Submitted for publication.
Jajcay, N., Hlinka, J., Kratsov, S., Tsonis, A.A., Palus, M., 2016. Time scales of the European surface air temperature variability: the role of the 7-8 year cycle. Geophys. Res. Lett. https://doi.org/10.1002/2015GL067325.
Kim, K.-Y., Hamlington, B.D., Na, H., 2015. Theoretical foundation of CSEOF analysis for geophysical and climatic variables: concepts and examples. Earth-Sci. Rev. 150, 201–218. https://doi.org/10.1016/j.earscirev.2015.06.003.
Legeais, J.F., Ablain, M., Zawadzki, L., Zuo, H., Johannessen, J.A., Scharffenberg, M.G., Fenoglio-Marc, L., Fernandes, J., Andersen, O.B., Rudenko, S., Cipollini, P., Quartly, G.D., Passaro, M., Cazenave, A., Benveniste, J., 2018. An improved and homogeneous altimeter sea level record from the ESA climate Change Initiative. Earth Syst. Sci. Data 10, 281–301. https://doi.org/10.5194/essd-10-281-2018.
Meyer, P.G., Kantz, H., 2019. Single decomposition of European temperature variability capturing the variance from days to a decade. Clim. Dyn. 53, 6909–6917. https://doi.org/10.1007/s00382-019-04965-0.
Nerem, R.S., Chambers, D.P., Choe, C., Mitchum, G.T., 2010. Estimating mean sea level change from the TOPEX and Jason Altimeter Missions. Mar. Geod. 33 (sup1), 435–446. https://doi.org/10.1080/01490419.2010.491031.
Nerem, R.S., Beckley, B.D., Fasullo, J., Hamlington, B.D., Masters, D., Mitchum, G.T., 2018. Climate change driven accelerated sea level rise detected in the Altimeter Era. Proc. Natl. Acad. Sci. 15 (9), 2022–2025. https://doi.org/10.1073/pnas.1717312115.
Palanisamy, H., Meyssignac, B., Cazenave, A., Delcroix, T., 2015. Is the anthropogenic sea level fingerprint already detectable in the Pacific Ocean? Environmental Research Letters 10. https://doi.org/10.1088/1748-9326/10/12/124010, 124010.
Peltier, W.R., 2004. Global glacial isostasy and the surface of the ice-age Earth: the ICE-5G (VM2) model and GRACE. Annu. Rev. Earth Planet. Sci. 32, 111.
Piecuch, C.G., Quinn, K.J., 2016. El Niño, La Niña, and the global sea level budget. Ocean Sci. 12, 1165–1177. https://doi.org/10.5194/os-12-1165-2016.
VanderPlas, J.T., 2018. Understanding the lomb-scargle periodogram. Astr. J. Suppl. Ser. 236 (1).
Veng, T., Andersen, O.B., 2020. Consolidating sea level acceleration estimates from satellite altimetry. Adv. Space Res. https://doi.org/10.1016/j.asr.2020.01.016 in press.
Von Schuckmann, K., et al., 2020. Copernicus marine service ocean state report, issue 4. J. Oper. Oceanogr. 13 (sup 1), S1–S172. https://doi.org/10.1080/1755876X.2020.1785097.
Watkins, A., Fu, Y., Gross, R., 2018. Earth's subdecadal angular momentum balance from deformation and rotation data. Sci. Rep. 8, 113761. https://doi.org/10.1038/s41598-018-32043-8.
Watson, C.S., White, N.J., Church, J.A., King, M.A., Burgette, R.J., Legresy, B., 2015. Unabated global mean sea-level rise over the world satellite altimeter era. Nat. Clim. Chang. 5 (6), 565–568. https://doi.org/10.1038/nclimate2635.
Wu, C., Yu, J.Z., 2018. Evaluation of linear regression techniques for atmospheric applications: the importance of appropriate weighting. Atmos. Meas. Tech. 11, 1233–1250. https://doi.org/10.5194/amt-11-1233-2018.
Yi, S., Heki, K., Qian, A., 2017. Acceleration in the global mean sea level rise: 2005-2015. Geophys. Res. Lett. 44, 11905–11913. https://doi.org/10.1002/2017GL076129.
Zhang, X., Church, J.A., 2012. Sea level trends, interannual and decadal variability in the Pacific Ocean. Geophys. Res. Lett. 39 https://doi.org/10.1029/2012GL053240. L21701.